DOI: 10.1002/ejic.201100224

Complete Two-Step Spin-Transition in a 1D Chain Iron(II) Complex with a 110-K Wide Intermediate Plateau

Wolfgang Bauer,[a,b] Toni Pfaffeneder,[b] Klaus Achterhold,[c] and Birgit Weber*[a]

Keywords: Spin crossover / Coordination polymers / Magnetic properties / Moessbauer spectroscopy / Iron

Three new spin crossover compounds [FeL1(azpy)] (**1**), [FeL1(azpy)]·toluene [**1**(tol)] and [FeL2(azpy)] (**2**), where L1 and L2 are the tetradentate $N_2O_2^{2-}$ coordinating Schiff base like ligands {diethyl (*E*,*E*)-2,2′-[1,2-phenyl-bis(iminomethylidyne)]bis[3-oxobutanoate]-(2-)-*N*,*N*′,O^3,$O^{3'}$} and {dimethyl (*E*,*E*)-2,2′-[1,2-phenyl-bis(iminomethylidyne)]bis[3-oxobutanoate]-(2-)-*N*,*N*′,O^3,$O^{3'}$}, respectively, and azpy = 4,4′-azopyridine are presented. All compounds have been investigated by using *T*-dependent susceptibility measurements, and different types of spin transitions are observed. In the case of **1** and **2**, intermediate plateaus ($\gamma_{HS} \approx 0.5$) with widths of 110 and 75 K, respectively, were observed, while for **1**(tol) a gradual spin transition is obtained. Upon heating of **1**(tol) above 390 K, a loss of the included solvent molecule toluene is observed, which results in a two-step spin transition of the tempered sample similar to that of **1**. Mössbauer spectra of **1**, **1**(tol) and the tempered sample **1**(temp) reveal two different iron(II) sites in the low-spin (LS) state for all three samples. *T*-dependent Mössbauer spectra indicate that the inequivalent iron centres are one but not the only reason for the wide plateau of **1**. Results from X-ray structure analysis of **1** in the region of the plateau show the presence of two inequivalent iron centres, of which one is in the high-spin (HS) state and one in the low-spin state. The 1D chains of alternating HS and LS iron centres are arranged in a parallel manner within one layer; between the different layers, the direction of the chains rotates by 90° relative to the previous one. This cross-linked arrangement with an interlocking of the layers is most likely the reason for the appearance of the wide plateau.

Introduction

Spin-transition complexes (spin crossover, SCO) are an interesting class of compounds that can be switched on the molecular level between two different states by the use of external perturbations such as temperature, pressure or electromagnetic radiation. The SCO bistability is one of the most promising aspects for new electronic devices in molecular memories and switches, as the switching progress is associated with a change in the magnetic and physical properties, which can be easily detected by different means.[1,2] Of the possible types of spin transition, stepwise transitions between three or more states attracted the interest of several research groups, because of versatile switching possibilities.[3–5] To date, three different possibilities are discussed for describing step-wise spin transitions. One is related to dinuclear complexes and explained with the formation of [HS–HS], [HS–LS] and [LS–LS] spin pair states (where HS and LS represent the local high-spin and low-spin states of the dinuclear species). These states could directly be monitored, for example, by Mössbauer spectroscopy and switched selectively by different wavelengths.[3–6] An interplay between intramolecular magnetic exchange interactions and spin transition is made responsible for the step in the transition curve.[3–5,7] Another possibility to have a multistep spin transition is attributed to two (or more) different SCO sites, each undergoing a transition at different temperatures.[8–10] We presented a mononuclear system clearly belonging to this category, with a large plateau in the range 225–125 K and at $\gamma_{HS} \approx 0.25$. The reason for this behaviour is four inequivalent iron(II) sites in the crystal lattice with slightly different chemical surroundings, which result from an additional distorted 4-cyanopyridine molecule, in combination with strong π–π interactions between two neighbouring molecules.[9] Finally, there are examples of mononuclear complexes with a unique crystallographic iron(II) site in the HS state, at which the effects of ferromagnetic-type long-range and antiferromagnetic-type short-range interactions of an elastic origin induce a crystallographic phase transition that is responsible for steps in the transition curve.[11] Those crystallographic phase transitions are accompanied or triggered by a symmetry breaking

[a] Inorganic Chemistry II, Universität Bayreuth, Universitätsstraße 30, NW I, 95440 Bayreuth, Germany
Fax: +49-921552157
E-mail: weber@uni-bayreuth.de
[b] Center for Integrated Protein Science Munich at the Department Chemie, Ludwig-Maximilians-Universität München, Butenandtstr. 5-13 (Haus F), 81377 München, Germany
[c] Technische Universität München, Physik-Department E17, James-Franck Straße 1, 85747 Garching, Germany
Supporting information for this article is available on the WWW under http://dx.doi.org/10.1002/ejic.201100224.

in the crystal, which leads to two[12] or even more[13] intermediate phases, each accompanied by a spin-state change in the system. Different theoretical models were developed to describe the HS/LS ordering in such systems.[14]

Recently, the first two examples for a 1D polymeric material undergoing a two-step spin transition were presented by Neville, Murray and co-workers.[15] In the case of the first complex, the two-step behaviour can be related to two different iron(II) environments, whereas for the second complex with a slightly broader intermediate plateau (IP), only one distinct iron(II) site is observed at all temperatures. Systematic investigations on a series of 1D chain compounds with Schiff base like equatorial ligands used in our group lead to different types of spin transition.[16,17] Two different reasons were identified to be responsible for the step in the transition curve: inequivalent iron sites in the HS state or, if a single iron site is observed in the HS state, a change in symmetry leading to a phase with two iron sites (HS, LS) in the region of the plateau. An analysis of the intermolecular interactions revealed that a pronounced zigzag structure of the 1D chain combined with restraining interactions between the 1D chains (several short contacts) favour such a phase transition and lead to steps in the transition curve.[16]

In this work, we present two iron(II) 1D coordination polymers [FeL1(azpy)] (**1**) and [FeL2(azpy)] (**2**) whose solvent-free samples show a complete two-step spin transition with an >75-K wide IP around room temperature. The SCO of the solvent-containing sample [FeL1(azpy)]·toluene [**1**(tol)] is gradual but can be transferred to a two-step transition by solvent-loss. The complexes are based on a N_2O_2 coordinating Schiff base like ligand system that was demonstrated to be highly suitable for the synthesis of iron(II) SCO complexes if combined with *N*-heterocycles as axial ligands.[18,19] 4,4′-Azopyridine (azpy) was used as a bridging axial ligand. In Scheme 1, the formula of the used ligands and the general synthesis route is given.

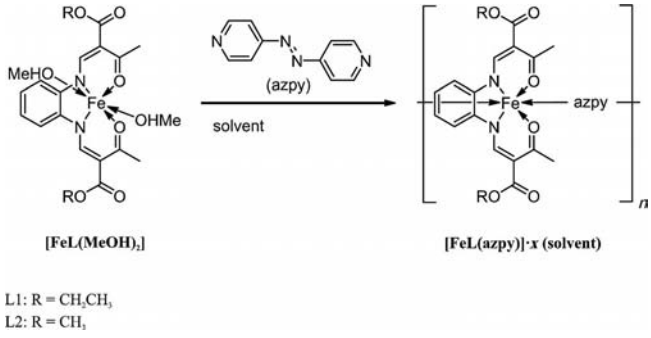

Scheme 1. General synthesis of the 1D octahedral iron(II) coordination polymers discussed in this work.

Results and Discussion

Magnetic Measurements

The thermal dependence of the product $\chi_M T$ (χ_M is the molar susceptibility and T the temperature) for **1** and **1**(tol) is displayed in Figure 1. Both compounds reach their maximum $\chi_M T$ values not before 400 K. Compound **1** shows a complete two-step SCO with a wide IP, whereas **1**(tol) shows a complete gradual SCO at first, but after being heated to 400 K, the SCO behaviour changes into a two-step transition similar to that of **1**. The room temperature $\chi_M T$ value of **1** is 1.63 $cm^3 K mol^{-1}$ in the region expected for an approximately 50:50 mixture of LS and HS iron centres. The maximum $\chi_M T$ value of 2.99 $cm^3 K mol^{-1}$, indicative of iron(II) in the high-spin state, is obtained when **1** is heated to 400 K. Upon cooling, the $\chi_M T$ values decrease gradually in the temperature range 400–295 K to a value of 1.63 $cm^3 K mol^{-1}$, which indicates that half of the iron(II) sites are in the HS state (γ_{HS} = 0.5). The $T_{1/2}(1)$ value of this step is 326 K. In the whole temperature range 295–185 K, the $\chi_M T$ values slightly decrease by about 0.27 $cm^3 K mol^{-1}$ to a value of 1.36 $cm^3 K mol^{-1}$, which results overall in a 110-K wide IP. Below 185 K, the $\chi_M T$ values decrease rapidly to attain a minimum value of 0.08 $cm^3 K mol^{-1}$ at 128 K, indicative of iron(II) in its diamagnetic LS state. Upon further cooling, the $\chi_M T$ values remain approximately constant. The $T_{1/2}(2\downarrow)$ value of the second step is 152 K, which means a separation distance between both $T_{1/2}$ values of 174 K. Upon heating, the $\chi_M T$ values remain approximately constant up to 150 K, followed by an abrupt increase, with $T_{1/2}(2\uparrow)$ = 159 K. This results in a thermal hysteresis loop with an average width

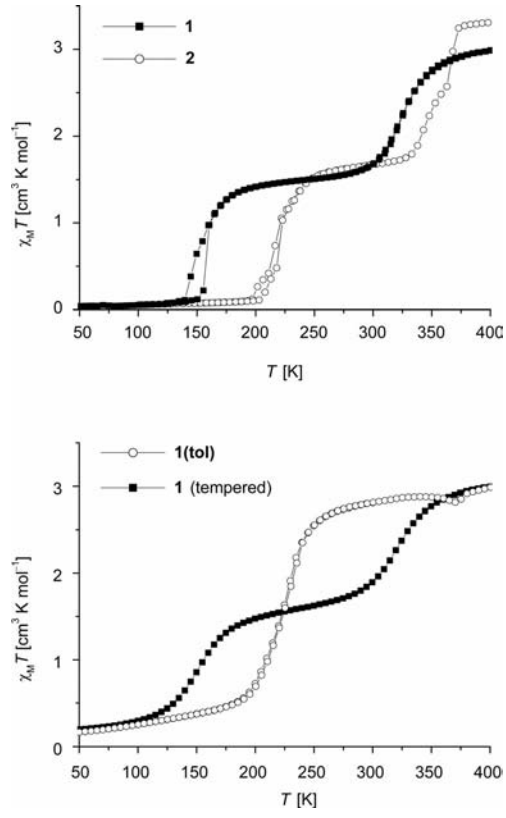

Figure 1. Plot of the $\chi_M T$ product vs. T over the temperature range 50–400 K. Top: compound **1** and compound **2**. Bottom: compound **1**(tol) and **1**(tol) after heating to 400 K [**1**(temp)].

of 7 K. Above 160 K, the curve progression of the heating and cooling mode is identical. The heating and cooling cycle could be repeated several times.

The room temperature $\chi_M T$ value of **1**(tol) is 2.81 $cm^3 K mol^{-1}$, which indicates that almost all iron(II) sites are in the HS state. Upon cooling, the $\chi_M T$ values decrease, gradually then more rapidly then again gradually, to attain a minimum value of 0.16 $cm^3 K mol^{-1}$ at 50 K, indicative of iron(II) in the LS state. A thermal hysteresis is not observed upon heating. Above 300 K, the $\chi_M T$ values slightly increase to attain a maximum of 2.88 $cm^3 K mol^{-1}$ at 340 K. The $T_{1/2}$ value of this SCO is 222 K. Further heating causes a decrease to a local minimum of 2.81 $cm^3 K mol^{-1}$ at 370 K, before the $\chi_M T$ values finally increase up to 2.99 $cm^3 K mol^{-1}$ at 400 K. This irregularity at about 370 K is probably due to the loss of the uncoordinated toluene molecule. This assumption is strengthened when measuring the tempered sample [**1**(temp)] in the cooling mode. The previously obtained gradual SCO behaviour is not observed, but a step-wise spin transition curve very similar to that of the solvent-free compound **1**. With a maximum $\chi_M T$ value of 2.99 $cm^3 K mol^{-1}$ at 400 K and a minimum value of 0.16 $cm^3 K mol^{-1}$ at 50 K, the two-step SCO of **1**(temp) is complete, too. Marginal differences can be found by looking at the $T_{1/2}$ values of **1**(temp) [$T_{1/2}(1)$ = 320 K and $T_{1/2}(2)$ = 150 K], which are slightly lower than the values of **1** [$T_{1/2}(1)$ = 326 K and $T_{1/2}(2)$ = 152 K]. Further, the SCO curve progression of **1**(temp) is more gradual. Thermogravimetric measurements of **1**(tol) confirm the presumption that the loss of toluene has to be responsible for the different spin-transition behaviour. At 388 K (boiling point toluene: 384.2 K), **1**(tol) has lost 13.7% of its mass (theory for one toluene molecule: 12.8%), which is consistent with the result from elemental analysis. The differences between the transition curves of **1** and **1**(temp) are most likely because of differences in the particle size (grinding effects).

The thermal dependence of the product $\chi_M T$ for compound **2** is also plotted in Figure 1. Overall, **2** provides a complete two-step SCO that reaches its maximum $\chi_M T$ value of 3.30 $cm^3 K mol^{-1}$, indicative of HS iron(II), not before 375 K. However, a closer look reveals an irregular curve progression, which could be confirmed by calculation of the first derivation of the curve (Supporting Information, Figure S1). Altogether four maxima at different temperatures were found, which correspond to four inflection points in the $\chi_M T$ vs. T plot. Starting at 400 K, the $\chi_M T$ values remain approximately constant between 400 and 370 K. Between 370 and 325 K, the $\chi_M T$ values rapidly decrease to attain a minimum value of 1.72 $cm^3 K mol^{-1}$, which indicates that half of the iron(II) centres are in the HS state. The $T_{1/2}(1)$ value of this step is 365 K. During this first step, an anomaly is observed with an inflection point at 340 K. In the temperature range 325–250 K, the $\chi_M T$ values slightly decrease by about 0.18 $cm^3 K mol^{-1}$ to a value of 1.54 $cm^3 K mol^{-1}$, which results in an 75-K wide IP. Between 250 and 190 K, the $\chi_M T$ values rapidly decrease to attain a minimum value of 0.09 $cm^3 K mol^{-1}$, indicative of iron(II) in the LS state. The $T_{1/2}(2\downarrow)$ value of this step is 214 K. During this second step another anomaly, similar to the previous one, is observed with an inflection point at 199 K. Below 190 K, the $\chi_M T$ values remain approximately constant. Comparison with the heating mode reveals a 4-K wide hysteresis loop for the second step, with a $T_{1/2}(2\uparrow)$ value of 218 K.

Mössbauer Spectroscopy

The two-step SCO of **1** was followed by Mössbauer spectroscopy in the temperature range 80–300 K in the heating and cooling mode. For comparison, the Mössbauer spectra of **1**(tol) and **1**(temp) were recorded at selected temperatures. Selected spectra at different temperatures of the three

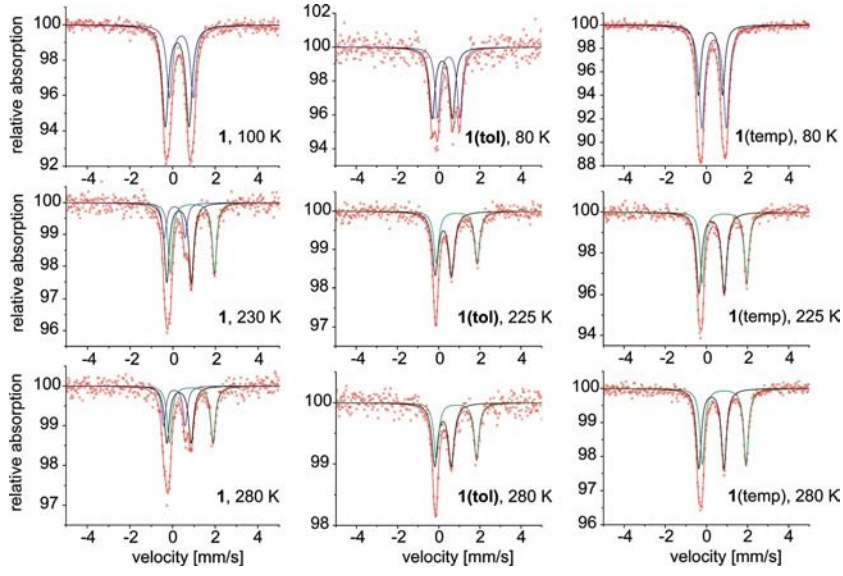

Figure 2. Mössbauer spectra of **1**, **1**(tol) and **1**(temp) at different temperatures: black and blue: LS and green: HS.

Table 1. Representative least-squares-fitted Mössbauer data for **1**, **1**(tol) and **1**(temp).

Compound	low-spin 1			low-spin 2			high spin		
	δ[a]	ΔE_Q[a]	Γ[a]	δ[a]	ΔE_Q[a]	Γ[a]	δ[a]	ΔE_Q[a]	Γ[a]
					80 K				
1 (100 K)	0.33(1)	1.11(1)	0.35(2)	0.53(1)	1.12(1)	0.32(2)			
1(tol)	0.30(1)	0.98(1)	0.33(3)	0.61(2)	1.07(2)	0.30(3)			
1(temp)	0.31(1)	1.17(1)	0.29(2)	0.49(1)	1.19(1)	0.34(1)			
					225 K				
1 (230 K)	0.19(1)	0.98(2)	0.25(4)	0.40(1)	1.15(1)	0.27(2)	1.03(1)	2.07(1)	0.25(2)
1(tol)	0.34(1)	0.79(2)	0.35(2)				0.99(1)	1.99(2)	0.29(2)
1(temp)	0.37(1)	1.22(1)	0.31(1)				0.99(1)	2.16(1)	0.26(1)
					280 K				
1	0.20(1)	1.01(2)	0.25(4)	0.41(1)	1.14(2)	0.29(3)	0.99(1)	2.05(1)	0.27(2)
1(tol)	0.31(1)	0.81(2)	0.34(3)				0.96(1)	1.96(2)	0.29(3)
1(temp)	0.35(1)	1.22(1)	0.30(1)				0.98(1)	2.14(1)	0.28(1)

[a] Isomer shifts [δ, mm s^{-1}] refer to α iron; ΔE_Q = quadrupole splitting [mm s^{-1}]; Γ = full width at half maximum of the Lorentzian lines [mm s^{-1}]. Statistical standard deviations are given in parentheses.

compounds are given in Figure 2, and the corresponding values of the Mössbauer parameters obtained by least-squares fitting are given in Table 1. A complete list of all *T*-dependent Mössbauer parameters and a detailed description of the interpretation of the Mössbauer spectra is given in the Supporting Information, Tables S1–S3 and Figures S2–S4.

At 80 K (**1**: until 150 K), the Mössbauer parameters of the three compounds are typical for octahedral iron(II) complexes of this ligand type in the LS state ($\Delta E_Q \approx 1.1$ cm^{-1}, $\delta = 0.3$–0.6 cm^{-1})[20–22] with no indication of a remaining HS fraction. The Mössbauer spectra of **1** and **1**(temp) are very similar, both consisting of a quadrupole-split doublet with a wide line width, which suggests two (or more) inequivalent iron centres. In the case of **1**(tol), two quadrupole split doublets of two inequivalent iron centres are clearly visible. Upon heating, a new quadrupole split doublet appears with parameters ($\Delta E_Q \approx 2.0$ cm^{-1}, $\delta \approx 1.0$ cm^{-1}) typical for iron(II) complexes in the HS state.[20–22]

At 280 K, the spin transition is not complete for all three compounds, in agreement with the outcomes from the susceptibility measurements. However, in the case of **1**(tol), a nearly complete spin transition would be expected that is not reflected in the spectrum at 280 K. Probably, during the long measurement time (one month at 280 K), a partial loss of the included toluene occurs. For **1**(tol) and **1**(temp) two quadrupole split doublets are observed, one is assigned to the HS and one to the LS state. This behaviour is expected for a step-wise SCO because of inequivalent iron centres. Despite this observation, in the case of **1**(tol) a one-step spin transition is observed. In the case of **1**, three quadrupole split doublets are clearly visible – two belong to the LS and one to the HS state. This is unexpected, as, in this case, a step-wise spin transition is observed. If inequivalent iron centres are responsible for the step, one would assume that at first one and then the second iron centre undergo spin transition. Thus, at the IP, one doublet for the HS state and one doublet for the LS state should be observed as described for **1**(tol). For the 1D chain compounds investigated here, the situation is more complex. Although the area of one of the LS doublets ($\Delta E_Q = 1.11$ cm^{-1}, $\delta = 0.33$ cm^{-1}) decreases at the beginning of the spin transition, it does not completely vanish, but instead the area of the second LS doublet ($\Delta E_Q = 1.12$ cm^{-1}, $\delta = 0.53$ cm^{-1}) starts to decrease, while the area of the HS doublet continuously increases. A good agreement between the transition curve obtained by Mössbauer spectroscopy and SQUID measurements is obtained as given in Figure 3. However, the inequivalent iron centres detected by Mössbauer spectroscopy in the LS state clearly cannot be the only reason for the wide IP in the transition curve of **1**, as they are also observed for **1**(tol) with a gradual spin transition.

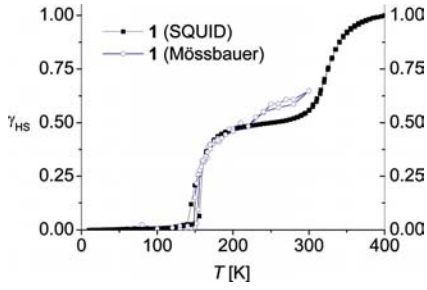

Figure 3. Thermal dependence of γ_{HS} of **1** obtained from Mössbauer spectroscopy and SQUID measurements.

X-ray Structure Analysis

Crystals suitable for X-ray structure analysis were obtained for compound **1**. Additionally, a few single crystals were obtained from a diluted toluene solution of **1**(tol) with the composition [FeL1(azpy)]·2toluene [**1**(2tol)]. The crystal structure of **1** was determined on the IP at 200 K and in the LS state at 130 K. Unfortunately, the crystallographic data of the LS structure were inferior, as twinning occurred upon phase transition while cooling down. As a result of technical limitations, a lower temperature was not access-

Table 2. Selected bond lengths [Å] and angles [°] for the inner coordination sphere of HS (S = 2) and LS (S = 0) iron centres of **1** (200 K) and **1**(2tol) (173 K).

	S	Fe–N_{eq}	Fe–O_{eq}	Fe–N(L_{ax})	O_{eq}–Fe–O_{eq}	L_{ax}–Fe–L_{ax}
1	2 Fe1	2.090(3) 2.083(3)	2.016(3) 2.006(3)	2.214(3) 2.283(3)	112.4(1)	176.1(1)
	0 Fe2	1.891(3) 1.903(3)	1.933(3) 1.934(3)	1.976(3) 2.001(3)[a]	87.6(1)	179.0(1)[a]
1(2tol)	2	2.046(5) 2.051(5)	1.991(4) 1.989(4)	2.209(5)[b] 2.217(5)	105.2(2)	177.1(2)[b]

Symmetry code: [a] –1 + x, y, –1 + z. [b] 1 + x, y, 1 + z.

ible, and therefore only the structure motif is presented here. The crystal structure of **1**(2tol) was determined at 173 K. The crystallographic data of the complexes are summarised in Table 5. Selected bond lengths and angles within the inner coordination sphere of the iron(II) ion are summarised in Table 2. ORTEP drawings of the asymmetric units of **1** (200 K) and **1**(2tol) are given in Figure 4, the atom numbering scheme is indicated. In Figure 5, the asymmetric unit of **1** in the LS state is shown. For both materials, structure analysis reveals an octahedral iron(II) N_4O_2 environment consisting of one equatorially coordinated Schiff base like ligand with N_2O_2 binding sites and two axially coordinated azpy ligands bound through terminal pyridyl groups. Each azpy ligand bridges two iron(II) centres to form infinite 1D chains.

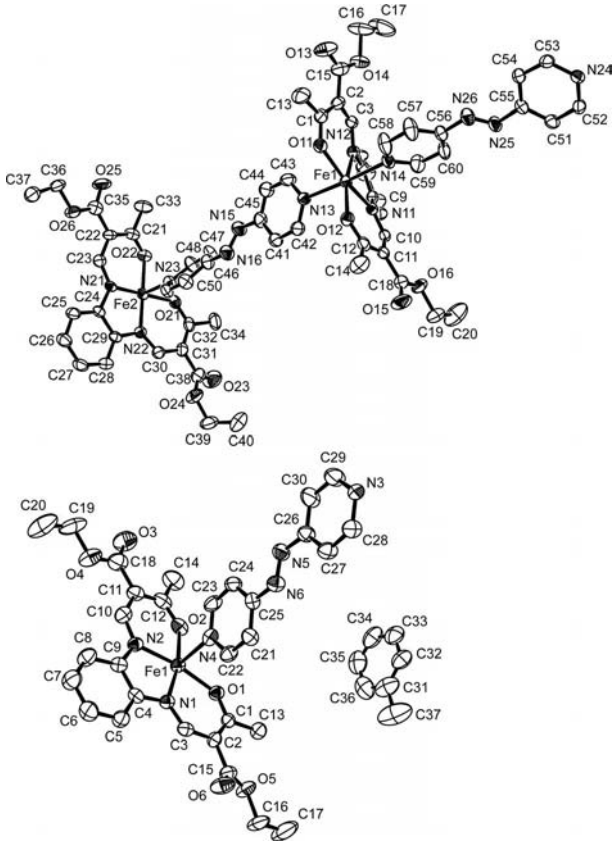

Figure 4. ORTEP drawings of the asymmetric units; top: **1** (200 K), bottom: **1**(2tol) (173 K). Hydrogen atoms as well as both disordered half occupied toluene molecules of **1**(2tol) have been omitted for clarity. Displacement ellipsoids are shown at the 50% probability level.

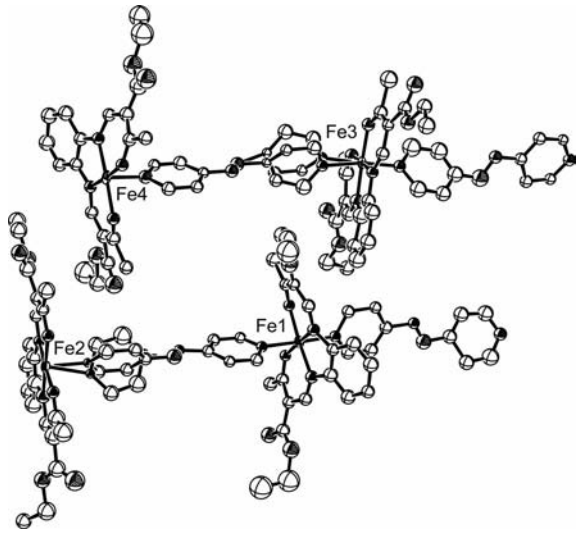

Figure 5. Asymmetric unit of the LS structure motif of **1** (130 K) with the inequivalent iron(II) centres numbered. Hydrogen atoms have been omitted for clarity. Displacement ellipsoids are shown at the 50% probability level.

Compound **1** crystallises at room temperature in the region of the IP with the orthorhombic space group $P2_12_12_1$. The asymmetric unit contains two crystallographically distinct iron(II) centres, one can be assigned to iron(II) in the HS state (Fe1) and one to iron(II) in the LS state (Fe2). The averaged metal–ligand distances around the inner coordination sphere of Fe1 (Fe1–N_{eq}: 2.09 Å, Fe1–O_{eq}: 2.01 Å, Fe1–N_{ax}: 2.25 Å) indicate a distorted, axially elongated octahedral environment, typical for HS iron(II) of this ligand type.[9,17,18,20,23] The averaged metal–ligand distances in the [FeN_4O_2] coordination core of Fe2 (Fe2–N_{eq}: 1.90 Å, Fe2–O_{eq}: 1.93 Å, Fe2–N_{ax}: 1.99 Å) are about 10% shorter than those for the HS state, as discussed in the literature for iron(II) SCO complexes.[2] Especially, the pronounced reduction of the Fe–N_{ax} distance (0.26 Å) in the direction of a more regular octahedral environment is indicative of LS iron(II). The O_{eq}–Fe–O_{eq} angle, the so called bite of the ligand, is another characteristic tool to determine the spin state of the central iron(II) ion for this type of complex, as it changes from about 110° in the HS state to about 90° in the LS state.[19] The bite angle for Fe1 (112°) suggests that it is clearly in the HS state and that for Fe2 (88°) indicates that it is clearly in the LS state.

Analysis of the polymeric structure shows the formation of infinite one-dimensional chains with the base vector [1 0 1]. Along the chains, an alternating arrangement of HS

and LS iron(II) centres is observed, which results in a mixed spin state with $\gamma_{HS} \approx 0.5$, in agreement with the magnetic measurements. The intrachain Fe1···Fe2 separation distances alternate between 13.2 Å and 13.3 Å. The azpy bridging ligand is strongly distorted, as the planes, which are spanned by the pyridyl rings, are twisted by about 37° and 53°, respectively, to each other. This overall leads to a straight-lined progression of the chains. In comparison to compound **1**, very similar coordination polymers with bpee and bpea as bridging ligands [bpee = bis(4-pyridyl)ethylene, bpea = bis(4-pyridyl)ethane], do not show distortions of the bridging ligand, and, therefore, a steplike chain progression is observed.[16,24] Upon cooling to 130 K, the symmetry of the system is reduced to the monoclinic space group $P2_1$. This structural phase transition is one explanation for the observed hysteresis at the second step of the spin-transition curve. It is also responsible for the decrease in quality of the data as the formation of domains is highly likely. The asymmetric unit contains four crystallographic distinct iron(II) centres (Figure 5). As can be seen from Table 3, the bite of the ligand of these iron(II) centres is in the range 85.5–92.8°, and, therefore, all iron(II) centres are definitely in the LS state.

Table 3. Bite of the ligand [°] of the four inequivalent iron(II) LS centres of the low-temperature structure of **1** at 130 K.

	Fe1	Fe2	Fe3	Fe4
O_{eq}–Fe–O_{eq}	91.9	85.8	88.5	92.8

Compound **1**(2tol) crystallises with the monoclinic space group $P2_1/c$. The asymmetric unit contains one crystallographic distinct iron(II) centre that is clearly in the HS state (Fe–N_{ax}: 2.21 Å, O_{eq}–Fe–O_{eq}: 105°). Together with the complex, uncoordinated solvent toluene is intercalated within the asymmetric unit; in addition to one regular toluene molecule there are two disordered half-occupied molecules. The composition of the crystals of **1**(2tol) significantly differs from the powder sample of **1**(tol) used for the SQUID and Mössbauer measurements. For those studies, only one toluene molecule is observed according to elemental analysis and DTG measurements. At 173 K, **1**(tol) is in the LS state according to SQUID and Mössbauer measurements, while the results from X-ray structure analysis of **1**(2tol) clearly indicate that the crystals are in the HS state at 173 K. Thus, the powder sample **1**(tol) and the crystals **1**(2tol) are clearly two different samples. An analysis of the polymeric structure of **1**(2tol) indicates the formation of infinite one-dimensional chains that propagate along the [1 0 1] direction. In contrast to that for compound **1**, the azpy ligand is not distorted and a steplike chain progression is observed. The intrachain Fe···Fe separation distance is 13.4 Å and is similar to that of **1**.

Intermolecular Investigations

In order to find possible reasons for the wide step in the transition curve of **1**, a detailed investigation of the intermolecular interactions and the molecule packing is necessary. As can be seen in Figure 6, compound **1** exhibits a layered structure. Within each layer, the chains are arranged in a parallel manner (Figure 6A). The shortest Fe···Fe separation distance between adjacent chains is 12.5 Å (Fe1···Fe2*) and no short contacts (contacts shorter than the sum of the van der Waals radii minus 0.19 Å) can be found. From symmetry reasons it follows that altogether four layers, A, B, C and D, can be observed in which the direction of the chains rotates by 90° relative to the previous layer (i.e. A: 0°; B: 90°; C: 180°; D: 270°) (Figure 4B, C), which results overall in a cross-linked arrangement of the chains. As a consequence, the chains in layer A and C run perpendicular to the chains in layers B and D, whereas the chains of A and C, respectively B and D, proceed in an (*anti*-)parallel fashion. The shortest separation distance of two iron centres between the layers of the perpendicular chains is 8.510 Å (Fe1···Fe2*). This is smaller than the shortest Fe···Fe separation distance between (*anti*-)parallel chains (9.26 Å, Fe1···Fe2*) and even much smaller than the shortest intrachain distance. This is, to the best of our knowledge, the first example of a 1D chain iron(II) SCO complex with a cross-linked arrangement of the single chains. This allows a very dense molecule packing and an interlocking of the layers, which could be one reason for the broadness of the IP.

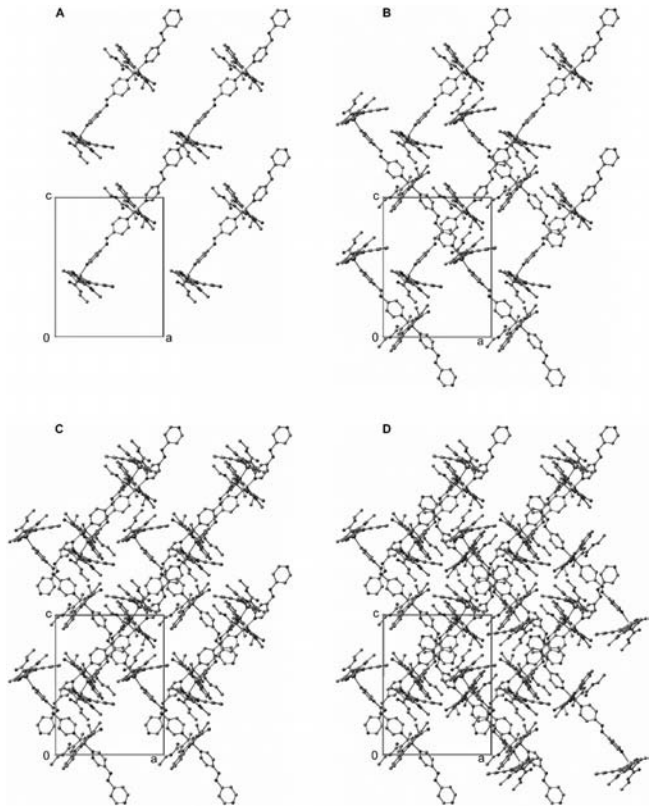

Figure 6. Packing of the polymer chains of **1** in the crystal projected in the *a*–*c* plane. For a better illustration of the layered, planar structure and the cross-linked arrangement of the chains, the content of the unit cell along the *b* axis is displayed layer-by-layer: (A) 20%, (B) 50%, (C) 70% and (D) 100%.

In general, a HS→LS transition in 1D chain compounds involves a relocation of the ligands towards the smaller LS molecule. If the Fe···Fe distances within the chain cannot follow the changes in Fe–L bonds because of restraining interactions, a stabilisation of a mixed HS/LS state can be observed.[16,25] We recently showed for 1D chain SCO complexes that a pronounced zigzag chain motif as well as a dense packing (intermolecular contacts shorter than the sum of the van der Waals radii) is responsible for restraining interactions between the chains and hence stabilise the mixed HS/LS state of a step.[16] In the case of compound **1**, the rigid packing and cross-linking of the chains probably counteracts the structural changes expected for a SCO system in a way similar to that observed for the zigzag 1D chains. During the HS→LS transition, a shortening of the bond lengths of one iron centre results in an elongation of the bond length of the neighbouring iron centre. The latter is involved in the stabilisation of the HS state at this iron centre and thus has a lower transition temperature. In fact, a number of intermolecular non-classical hydrogen bonds of the type C–H···O, which are listed in Table 4, can be found between the layers, which support this theory, as stabilised [HS···LS] pairs are built between adjacent chains. The hydrogen bond involving oxygen atom O13 (Fe1, HS) and hydrogen atom H50 (Fe2, LS) directly links a HS and a LS centre of adjacent perpendicular chains. In the same way, intermolecular [HS···LS] pairs are built between (*anti*-)parallel chains through the hydrogen bonds involving O25 (Fe2)/H41 (Fe1) and O15 (Fe1)/H53/54 (Fe2), respectively. To quantitatively describe the structural properties derived from X-ray structure analysis, we recently established the crystal contact index (CCI), which correlates the sum of intermolecular contacts with the strength of the cooperative effect.[17] The CCI scale proved to provide a good estimation to accompany the structural interpretation of spin-transition properties.[17] All short intermolecular contacts (shorter than sum of van der Waals radii) are listed in the Supporting Information (Table S2). The corresponding CCI value of 2.0 for compound **1** indicates a relatively high cooperativity (gradual SCO: <1.5), which is in line with the strong restraining interactions observed as a result of the cross linking of the chains and thus satisfactorily explains the wide IP. Because of the inferior structural data of the low-temperature structure of **1**, no far-reaching conclusions can be drawn with regard to the intermolecular short contacts. However, the structure motif of the molecule packing displayed in Figure 7 reveals a cross-linked arrangement of the chains as well.

Table 4. Bond lengths [Å] and angles [°] of intermolecular interactions with d(D···A) < R(D) + R(A) + 0.50, d(H···A) < R(H) + R(A) – 0.12 Å, ∠(D–H···A) > 100.0° for compound **1**.

1	d(D–H)	d(H···A)	d(D···A)	∠(D–H···A)
C(41)–H(41)···O(25)[a]	0.95	2.49	3.119(5)	123
C(50)–H(50)···O(13)[b]	0.95	2.49	3.262(5)	139
C(53)–H(53)···O(15)[c]	0.95	2.36	3.015(5)	126
C(54)–H(54)···O(15)[c]	0.95	2.52	3.085(5)	118
1(2tol)				
C(29)–H(29)···O(3)[d]	0.95	2.56	3.204(8)	126

Symmetry code: [a] $–x$, 1/2 + y, ½ – z. [b] ½ – x, 1 – y, –1/2 + z. [c] 1 – x, –1/2 + y, 3/2 – z. [d] $–x$, $–y$, 1 – z.

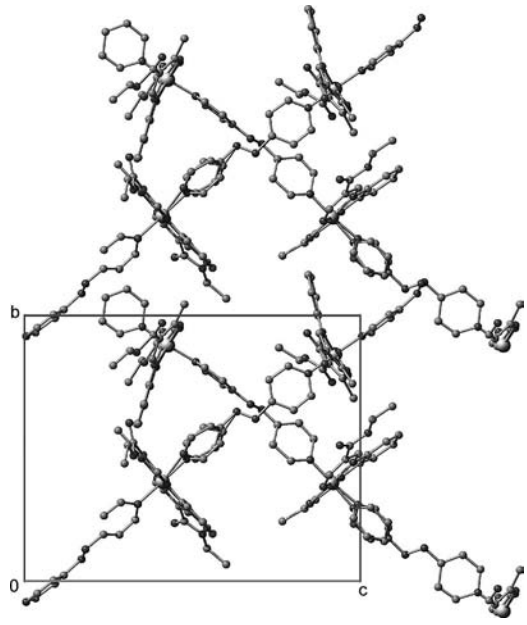

Figure 7. Packing of the polymer chains of the low-temperature structure motif of **1**, projected in the b–c plane. For reasons of clarity, only 50% of the contents of the unit cell along the a axis is displayed.

An excerpt of the molecule packing of **1**(2tol) is shown in Figure 8. In contrast to the packing of compound **1**, all chains run in a parallel fashion. The chains are arranged such that, between the bulky equatorial ligands and the smaller axial ligand, tubelike solvent accessible void volumes, reminiscent of molecule organic frameworks (MOFs), occur along the a and c axis in which the toluene molecules are intercalated (Figure 8). The shortest Fe···Fe separation distance between adjacent chains is 9.36 Å, shorter than that within the chain, but longer than that in **1**. As a consequence, the total number of short contacts between adjacent chains is smaller (Table S2) and only one non-classical hydrogen bond is observed, which involves the carbonyl oxygen atom O3 of the equatorial ligand and H29

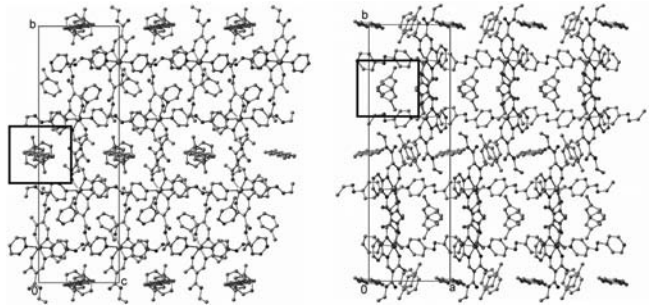

Figure 8. Packing of the polymer chains of **1**(2tol) in the crystal projected in the b–c plane (left) and the a–b plane (right). The tubelike void volumes with intercalated toluene are highlighted for clarification.

at the pyridyl ring of the axial ligand. As expected, the CCI of compound **1**(2tol) is relatively low (0.4), indicative of very weak cooperativity.[17] Unfortunately, we were not able to get enough crystals of **1**(2tol) to do any magnetic measurements.

Discussion

In order to reach an application for SCO compounds, a purposeful synthesis of such materials with defined properties is essential. Consequently, the question needs to be answered, why in the case of **1** and **2** such wide IPs are observed. The first suggestion from the X-ray structure analysis of **1** and the Mössbauer spectra would be that inequivalent iron centres are responsible for the different transition temperatures. However, the Mössbauer parameters of **1**(tol) are very similar to that of **1**, and here two inequivalent iron centres are clearly visible, although, in the magnetic measurements, only a gradual one-step spin transition is observed. The fact that the magnetic behaviour of **1**(tol) changes from gradual to steplike with the loss of toluene, similar to that seen in the $\chi_M T$ curve of **1**, leads to the assumption that the structure of **1**(tol) has to be more related to **1** than to **1**(2tol). Thus, it is highly probable that the special cross-linked arrangement of the 1D chains of **1** is responsible for the 110-K wide IP. As a very similar SCO is observed for **2**, a similar structure can be assumed that is probably related to the azpy ligand.

Next to the reasons for steps in the transition curve, it is important to investigate and understand the influence of solvent inclusions on the magnetic behaviour of SCO materials, as future applications as solvent-sensors are foreseeable. It is well known that solvent molecules intercalated into the crystal structure can either enhance or diminish cooperative effects and spin transition.[2] Networks of the stoichiometry $[Fe(bpee)_2(NCS)_2]$[26] and $[Fe(azpy)_2(NCS)_2]$[27] represent the first porous 2D grid metal-organic frameworks that exhibit a spin-state change triggered by host–guest chemistry, several further examples followed.[10,28] A similar dependence can be observed for the system described here: at room temperature, the solvent-free compound **1** is at the IP; if one toluene molecule is included, the complex switches to the HS state [**1**(tol)]. Similar effects were observed for related 1D chain SCO compounds of these Schiff base like equatorial ligands.[16] It appears that solvent effects are much more pronounced for 1D chain materials than for mononuclear complexes of the same ligand type. Further going investigations with regard to the reversibility of those effects are in progress.

Conclusions

In this work, we presented the synthesis and characterisation of new SCO coordination polymers with up to a 110-K wide IP. The complexes were investigated by using *T*-dependent susceptibility measurements, Mössbauer spectroscopy and X-ray diffraction. The results show that a clear assignment of the reasons for such a wide intermediate plateau is difficult. Although inequivalent iron centres are observed in the Mössbauer spectra and X-ray structures, their *T*-dependent behaviour indicates that this is not the only factor responsible for the plateau. The special cross-linked arrangement of the 1D chains of **1** also contributes to the spin-transition behaviour. The results provide a unique insight into the formation of a two-step spin transition and nicely show the influence of solvent molecules on SCO.

Experimental Section

Synthesis: If not described differently, all syntheses of the iron(II) complexes were carried out under argon by using Schlenk tube techniques. All solvents were purified as described in the literature[29] and distilled under argon. The syntheses of anhydrous iron(II) acetate,[30] ligand H_2L1,[31] ligand H_2L2[32] and the precursors $[FeL1(MeOH)_2]$[33] and $[FeL2(MeOH)_2]$[32] were published before. 4-Aminopyridine was purchased from Aldrich Chemical Co. and used as received. All complex syntheses were reproduced at least once.

4,4′-Azopyridine (azpy): 4,4′-Azopyridine was prepared by oxidative coupling of 4-aminopyridine and hypochlorite, by using an adaptation of Launay et al.[34] A cold solution of 4-aminopyridine (5.05 g, 53.7 mmol) in water (100 mL) was added dropwise to a NaOCl solution (300 mL of a 6.5% solution). The mixture was stirred at 5 °C as an orange precipitate formed. After completion of the addition, the reaction mixture was stirred for another 15 min. The precipitate was filtered off and washed with cold water. The aqueous phase was extracted three times with diethyl ether. The combined ether phases were dried on $MgSO_4$, and the solvents evaporated. The crude products were recrystallised from water to yield 4,4′-azopyridine as orange needles (yield: 1.70 g, 34%). ^{1}H NMR (270 MHz, $CDCl_3$, 25 °C, TMS): δ = 8.9 (m, 4 H, Ar-H), 7.7 (m, 4 H, Ar-H) ppm. MS [DEI-(+), 70 eV]: *m*/*z* (%) = 184 (55) [M^+], 78 (100) [$C_5H_4N^+$]. $C_{10}H_8N_4$ (184.20): calcd. C 65.21, H 4.38, N 30.42; found C 64.67, H 4.20, N 30.18.

[FeL1(azpy)] (1): $[FeL1(MeOH)_2]$ (0.26 g, 0.51 mmol) and azpy (0.47 g, 2.57 mmol) were dissolved in ethanol (40 mL) and heated to reflux for 4 h. Compound **1** precipitated from the reaction mixture after 4 d at room temperature in the form of black crystals, which were filtered off, washed with ethanol and dried in vacuo (yield: 0.25 g, 78%). IR (KBr): $\tilde{\nu}$ = 1686 (COO), 1566 (CO) cm^{-1}. MS [DEI(+), 70 eV]: *m*/*z* (%) = 442 (20) [$FeL1^+$], 184 (48) [$azpy^+$]. $C_{30}H_{30}FeN_6O_6$ (626.44): calcd. C 57.52, H 4.83, N 13.42; found C 57.16, H 4.70, N 12.91.

[FeL1(azpy)]·toluene [1(tol)]: $[FeL1(MeOH)_2]$ (1.11 g, 2.19 mmol) and azpy (2.02 g, 11.0 mmol) were dissolved in toluene (60 mL) and warmed to 80 °C for 1 h. Compound **1**(tol) was obtained after 1 d at room temperature in the form of a black microcrystalline precipitate, which was filtered off from the reaction mixture, washed with toluene and dried in vacuo. (yield: 1.41 g, 90%). IR (KBr): $\tilde{\nu}$ = 1685 (COO), 1566 (CO) cm^{-1}. MS [DEI(+), 70 eV]: *m*/*z* (%) = 442 (100) [$FeL1^+$], 184 (25) [$azpy^+$]. $C_{30}H_{30}FeN_6O_6{\cdot}C_7H_8$ (718.58): calcd. C 61.84, H 5.33, N 11.70; found C 62.79, H 5.41, N 11.32. The mother liquor of **1**(tol) was allowed to stand at 4 °C. After two months, black crystals with the composition **1**(2tol) had formed, which were of sufficient quality for crystal structure analysis.

Table 5. Crystallographic data of iron(II) coordination polymer **1** and **1**(2tol).

	1 (HS–LS)	**1** (LS)	**1**(2tol)
Formula	$C_{60}Fe_2H_{60}N_{12}O_{12}$	$C_{120}H_{121}Fe_4N_{24}O_{24}$	$C_{44}H_{46}FeN_6O_6$
M_r [g mol^{-1}]	1252.90	2506.81	810.72
Crystal system	orthorhombic	monoclinic	monoclinic
Space group	$P2_12_12_1$	$P2_1$	$P2_1/c$
a [Å]	16.2024(4)	17.8442(7)	11.2681(4)
b [Å]	17.8809(4)	16.1027(7)	33.9573(11)
c [Å]	20.8774(5)	20.3955(8)	11.1503(4)
α [°]	90.00	90.00	90.00
β [°]	90.00	90.614(2)	106.2810(10)
γ [°]	90.00	90.00	90.00
V [Å^3]	6048.5(2)	5860.1(4)	4095.4(2)
Z	4	2	4
$\rho_{calcd.}$ [g cm^{-3}]	1.376	1.421	1.315
μ [mm^{-1}]	0.551	0.569	0.424
θ range [°]	3.2–25.3	3.2–25.4	3.26–23.50
λ [Å]	0.71073	0.71073	0.71073
T [K]	200	130	173
GOF	1.022	1.07	1.059
$R1$,[a] $wR2$[b] [$I > 2\sigma(I)$]	0.0443, 0.0948	0.1544, 0.3882	0.0784, 0.2085
$F(000)$	2608	2610	1704
Reflections collected	38753	34133	17933

[a] $R1 = \Sigma||F_o| - |F_c||/\Sigma|F_o|$. [b] $wR2 = \{\Sigma[w(F_o^2 - F_c^2)^2]/\Sigma w(F_o^2)^2\}^{1/2}$, $w = 1/[\sigma^2(F_o^2) + (aP)^2 + bP]$, where $P = [F_o^2 + 2(F_c^2)]/3$.

[FeL2(azpy)] (2): [FeL2(MeOH)$_2$] (0.30 g, 0.63 mmol) and azpy (0.59 g, 3.20 mmol) were dissolved in methanol (20 mL) and heated to reflux for 1 h. After 16 h at 4 °C, **2** precipitated from the reaction mixture in the form of a black, microcrystalline solid, which was filtered off, washed with methanol and dried in vacuo (yield: 0.14 g, 37%). IR (KBr): $\tilde{\nu}$ = 1692 (COO), 1567 (CO) cm^{-1}. MS [DEI(+), 70 eV]: *m*/*z* (%) = 414 (100) [FeL2$^+$], 184 (35) [azpy$^+$]. $C_{28}H_{26}FeN_6O_6$ (598.39): calcd. C 56.20, H 4.38, N 14.04; found C 55.81, H 4.41, N 13.99.

Magnetic Measurements: Magnetic susceptibility data were collected with a Quantum Design MPMSR2 SQUID magnetometer under an applied field of 0.5 T over the temperature range 50–400 K in the settle mode. All samples were placed in gelatine capsules held within plastic straws. The data were corrected for the diamagnetic magnetisation of the ligands, which were estimated by using tabulated Pascal's constants, and of the sample holder.

Mössbauer Spectra: Mössbauer spectra have been recorded by using a conventional Mössbauer spectrometer operating in a sinusoidal velocity profile. The sample was placed in a bath cryostat (Cryo Industries of America Inc., Model 11CC).

Differential Thermogravimetry: The thermal behaviour was studied by using a Setaram TG-92 equipped with a protected DTA-TG rod. The measurement was conducted under a streaming Helium atmosphere at a scan rate of 10 K min^{-1} by using 100-mL alumina crucibles.

X-ray Crystallography: The intensity data of **1** and **1**(2tol) were collected on a Nonius Kappa CCD diffractometer by using graphite-monochromated Mo-K_a radiation. The data were corrected for Lorentz and polarisation effects. The structure was solved by direct methods (SIR 97)[35] and refined by full-matrix least-square techniques against F_0^2 (SHELXL-97).[36] The hydrogen atoms were included at calculated positions with fixed displacement parameters. All non-hydrogen atoms were refined anisotropically. ORTEP-III[37] was used for the structure representation, SCHAKAL-99[38] for the representation of the molecule packing. Cell parameters and refinement results are summarised in Table 5. CCDC-821162 (**1**, 200 K) and CCDC-821163 [**1**(2tol)] contain the supplementary crystallographic data for this paper. These data can be obtained free of charge from The Cambridge Crystallographic Data Centre via www.ccdc.cam.ac.uk/data_request/cif.

Supporting Information (see footnote on the first page of this article): The details for the analysis of the Mössbauer spectra together with the least-squares-fitted Mössbauer data (Tables S1–S3 and Figures S2–S4), the analysis of short intermolecular contacts of **1** and **1**(2tol) (Table S4) and the first derivative of the $\chi_M T$ vs. T plot of **1**(tol) (Figure S1) are available.

Acknowledgments

This work has been supported financially by the Deutsche Forschungsgemeinschaft (WE 3546_4–1), the Fonds der Chemischen Industrie and the Center for Integrated Protein Science Munich (CIPSM).

[1] a) H. A. Goodwin, *Coord. Chem. Rev.* **1976**, *18*, 293–325; b) E. König in. *Struct. Bonding*, Springer Berlin/Heidelberg, **1991**, pp. 51–152; c) P. Gütlich, A. Hauser, H. Spiering, *Angew. Chem.* **1994**, *106*, 2109; *Angew. Chem. Int. Ed. Engl.* **1994**, *33*, 2024–2054; d) J. A. Real, A. B. Gaspar, M. C. Munoz, *Dalton Trans.* **2005**, 2062–2079; e) K. Nakano, N. Suemura, K. Yoneda, S. Kawata, S. Kaizaki, *Dalton Trans.* **2005**, 740–743; f) O. Sato, J. Tao, Y.-Z. Zhang, *Angew. Chem.* **2007**, *119*, 2200; *Angew. Chem. Int. Ed.* **2007**, *46*, 2152–2187; g) O. Sato, J. Tao, Y.-Z. Zhang, *Angew. Chem.* **2007**, *119*, 2200–2236; h) J. A. Kitchen, S. Brooker, *Coord. Chem. Rev.* **2008**, *252*, 2072–2092; i) K. S. Murray, *Eur. J. Inorg. Chem.* **2008**, 3101–3121; j) M. A. Halcrow, *Coord. Chem. Rev.* **2009**, *253*, 2493–2514; k) S. Brooker, J. A. Kitchen, *Dalton Trans.* **2009**, 7331–7340; l) K. S. Murray, *Aust. J. Chem.* **2009**, *62*, 1081; m) A. B. Koudriavtsev, W. Linert, *J. Struct. Chem.* **2010**, *51*, 335–365; n) O. Kahn, *Science* **1998**, *279(5347)*, 44–48; o) O. Kahn, C. Jay, J. Krober, R. Claude, F. Groliere. *Patent* **1995** EP0666561; p) J.-F. Létard, P. Guionneau, L. Goux-Capes in *Spin Crossover in Transition Metal Compounds I-III*, *Topics in Current Chemistry*, *233–235* (Eds.: P. Gütlich, H. Goodwin), Springer Berlin/Heidelberg, **2004**, pp. 221–249; q) A. Galet, A. B. Gaspar, M. C. Muñoz,

G. V. Bukin, G. Levchenko, J. A. Real, *Adv. Mater.* **2005**, *17*, 2949–2953.

[2] P. Gütlich, H. Goodwin (Eds.), *Spin Crossover in Transition Metal Compounds I-III*; Springer Berlin/Heidelberg, **2004**.

[3] J. A. Real, A. B. Gaspar, M. C. Muñoz, P. Gütlich, V. Ksenofontov, H. Spiering in *Spin Crossover in Transition Metal Compounds I-III*, *Topics in Current Chemistry*, *233–235* (Eds.: P. Gütlich, H. Goodwin), Springer Berlin/Heidelberg, **2004**, pp. 167–193.

[4] A. B. Gaspar, M. C. Munoz, J. A. Real, *J. Mater. Chem.* **2006**, *16*, 2522–2533.

[5] A. Bousseksou, G. Molnar, J. A. Real, K. Tanaka, *Coord. Chem. Rev.* **2007**, *251*, 1822–1833.

[6] S. Zein, S. A. Borshch, *J. Am. Chem. Soc.* **2005**, *127*, 16197–16201.

[7] A. Gaspar, M. Seredyuk, P. Gütlich, *J. Mol. Struct.* **2009**, *924–926*, 9–19.

[8] a) Y. Garcia, O. Kahn, L. Rabardel, B. Chansou, L. Salmon, J. P. Tuchagues, *Inorg. Chem.* **1999**, *38*, 4663–4670; b) G. S. Matouzenko, J.-F. Létard, S. Lecocq, A. Bousseksou, L. Capes, L. Salmon, M. Perrin, O. Kahn, A. Collet, *Eur. J. Inorg. Chem.* **2001**, 2935–2945; c) W. Hibbs, P. J. van Koningsbruggen, A. M. Arif, W. W. Shum, J. S. Miller, *Inorg. Chem.* **2003**, *42*, 5645–5653; d) P. Poganiuch, S. Decurtins, P. Guetlich, *J. Am. Chem. Soc.* **1990**, *112*, 3270–3278; e) A. Hauser, P. Gütlich, R. Hinek, H. Spiering, D. Schollmeyer, *Chem. Eur. J.* **1996**, *2*, 1427–1434; f) R.-J. Wei, B. Li, J. Tao, R.-B. Huang, L.-S. Zheng, Z. Zheng, *Inorg. Chem.* **2011**, *50*, 1170–1172.

[9] B. Weber, C. Carbonera, C. Desplances, J.-F. Létard, *Eur. J. Inorg. Chem.* **2008**, 1589–1598.

[10] B. Li, R.-J. Wei, J. Tao, R.-B. Huang, L.-S. Zheng, Z. Zheng, *J. Am. Chem. Soc.* **2010**, *132*, 1558–1566.

[11] a) M. Mikami, M. Konno, Y. Saito, *Chem. Phys. Lett.* **1979**, *63*, 566–569; b) N. Sasaki, T. Kambara, *Phys. Rev. B* **1989**, *40*, 2442; c) H. Spiering, T. Kohlhaas, H. Romstedt, A. Hauser, C. Bruns-Yilmaz, J. Kusz, P. Gütlich, *Coord. Chem. Rev.* **1999**, *190–192*, 629–647; d) V. Petrouleas, J.-P. Tuchagues, *Chem. Phys. Lett.* **1987**, *137*, 21–25; e) D. Boinnard, A. Bousseksou, A. Dworkin, J. M. Savariault, F. Varret, J. P. Tuchagues, *Inorg. Chem.* **1994**, *33*, 271–281.

[12] a) D. Chernyshov, M. Hostettler, K. W. Törnroos, H.-B. Bürgi, *Angew. Chem.* **2003**, *115*, 3955; *Angew. Chem. Int. Ed.* **2003**, *42*, 3825–3830; b) N. Huby, L. Guérin, E. Collet, L. Toupet, J.-C. Ameline, H. Cailleau, T. Roisnel, T. Tayagaki, K. Tanaka, *Phys. Rev. B* **2004**, *69*, 2; c) M. Yamada, H. Hagiwara, H. Torigoe, N. Matsumoto, M. Kojima, F. Dahan, J.-P. Tuchagues, N. Re, S. Iijima, *Chem. Eur. J.* **2006**, *12*, 4536–4549; d) S. Bonnet, M. A. Siegler, J. S. Costa, G. Molnar, A. Bousseksou, A. L. Spek, P. Gamez, J. Reedijk, *Chem. Commun.* **2008**, 5619–5621; e) M. Griffin, S. Shakespeare, H. J. Shepherd, C. J. Harding, J.-F. Létard, C. Desplanches, A. E. Goeta, J. A. K. Howard, A. K. Powell, V. Mereacre, Y. Garcia, A. D. Naik, H. Müller-Bunz, G. G. Morgan, *Angew. Chem. Int. Ed.* **2011**, *50*, 896–900.

[13] N. Bréfuel, H. Watanabe, L. Toupet, J. Come, N. Matsumoto, E. Collet, K. Tanaka, J.-P. Tuchagues, *Angew. Chem.* **2009**, *121*, 9468; *Angew. Chem. Int. Ed.* **2009**, *48*, 9304–9307.

[14] a) A. Bousseksou, J. Nasser, J. Linares, K. Boukheddaden, F. Varret, *J. Phys. I France* **1992**, *2*, 1381–1403; b) D. Chernyshov, H.-B. Bürgi, M. Hostettler, K. Törnroos, *Phys. Rev. B* **2004**, *70*, 9; c) M. Nishino, K. Boukheddaden, S. Miyashita, F. Varret, *Polyhedron* **2005**, *24*, 2852–2856.

[15] S. M. Neville, B. A. Leita, G. J. Halder, C. J. Kepert, B. Moubaraki, J.-F. Létard, K. S. Murray, *Chem. Eur. J.* **2008**, *14*, 10123–10133.

[16] W. Bauer, W. Scherer, S. Altmannshofer, B. Weber, *Eur. J. Inorg. Chem.* **2011**, 2803–2818.

[17] T. M. Pfaffeneder, S. Thallmair, W. Bauer, B. Weber, *New J. Chem.* **2011**, *35*, 691–700.

[18] B. Weber, *Coord. Chem. Rev.* **2009**, *253*, 2432–2449.

[19] B. Weber, E.-G. Jäger, *Eur. J. Inorg. Chem.* **2009**, 465–477.

[20] B. Weber, E. Kaps, J. Weigand, C. Carbonera, J.-F. Létard, K. Achterhold, F. G. Parak, *Inorg. Chem.* **2008**, *47*, 487–496.

[21] B. Weber, E. S. Kaps, J. Obel, K. Achterhold, F. G. Parak, *Inorg. Chem.* **2008**, *47*, 10779–10787.

[22] B. Weber, E. S. Kaps, C. Desplanches, J.-F. Létard, K. Achterhold, F. G. Parak, *Eur. J. Inorg. Chem.* **2008**, 4891–4898.

[23] B. Weber, E. Kaps, *Heteroat. Chem.* **2005**, *16*, 391–397.

[24] W. Bauer, B. Weber, *Inorg. Chim. Acta* **2009**, *362*, 2341–2346.

[25] a) A. B. Koudriavtsev, A. F. Stassen, J. G. Haasnoot, M. Grunert, P. Weinberger, W. Linert, *Phys. Chem. Chem. Phys.* **2003**, *5*, 3666–3675; b) A. B. Koudriavtsev, A. F. Stassen, J. G. Haasnoot, M. Grunert, P. Weinberger, W. Linert, *Phys. Chem. Chem. Phys.* **2003**, *5*, 3676–3683.

[26] J. A. Real, E. Andres, M. C. Munoz, M. Julve, T. Granier, A. Bousseksou, F. Varret, *Science* **1995**, *268(5208)*, 265–267.

[27] G. J. Halder, *Science* **2002**, *298(5599)*, 1762–1765.

[28] a) V. Niel, A. L. Thompson, M. C. Muñoz, A. Galet, A. E. Goeta, J. A. Real, *Angew. Chem.* **2003**, *115*, 3890; *Angew. Chem. Int. Ed.* **2003**, *42*, 3760–3763; b) S. M. Neville, G. J. Halder, K. W. Chapman, M. B. Duriska, P. D. Southon, J. D. Cashion, J.-F. Létard, B. Moubaraki, K. S. Murray, C. J. Kepert, *J. Am. Chem. Soc.* **2008**, *130*, 2869–2876.

[29] H. G. O. Becker, *Organikum: Organisch-chemisches Grundpraktikum*, Johann Ambrosius Barth, Berlin, **1993**.

[30] B. Weber, R. Betz, W. Bauer, S. Schlamp, *Z. Anorg. Allg. Chem.* **2011**, *637*, 102–107.

[31] L. Wolf, E.-G. Jäger, *Z. Anorg. Allg. Chem.* **1966**, *346*, 76–91.

[32] W. Bauer, T. Ossiander, B. Weber, *Z. Naturforsch. B* **2010**, *65*, 323–328.

[33] E.-G. Jäger, E. Häussler, M. Rudolph, A. Schneider, *Z. Anorg. Allg. Chem.* **1985**, *525*, 67–85.

[34] J. P. Launay, M. Tourrel-Pagis, J. F. Lipskier, V. Marvaud, C. Joachim, *Inorg. Chem.* **1991**, *30*, 1033–1038.

[35] A. Altomare, M. C. Burla, M. Camalli, G. L. Cascarano, C. Giacovazzo, A. Guagliardi, A. G. G. Moliterni, G. Polidori, R. Spagna, *J. Appl. Crystallogr.* **1999**, *32*, 115–119.

[36] a) G. Sheldrick, *Acta Crystallogr., Sect. A* **2008**, *64*, 112–122; b) G. Sheldrick, *SHELXL-97*, University of Göttingen, Göttingen, Germany, **1993**.

[37] a) L. Farrugia, *J. Appl. Crystallogr.* **1997**, *30*, 565; b) C. K. Johnson, M. N. Burnett, *ORTEP-III*, Oak-Ridge National Laboratory, Oak-Ridge, TN, **1996**.

[38] E. Keller, *Schakal-99*, University of Freiburg, Freiburg, Germany, **1999**.

Received: March 3, 2011
Published Online: June 17, 2011

